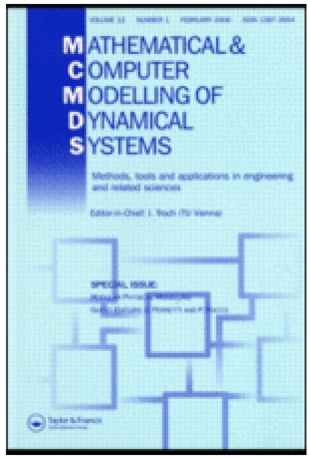

Explicit port-Hamiltonian FEM models for geometrically nonlinear mechanical systems

Journal:	*Mathematical and Computer Modelling of Dynamical Systems*
Manuscript ID	NMCM-2022-0010
Manuscript Type:	Research Article
Date Submitted by the Author:	04-Feb-2022
Complete List of Authors:	Thoma, Tobias; Technische Universitat Munchen, TUM School of Engineering and Design Kotyczka, Paul; Technische Universitat Munchen, TUM School of Engineering and Design
Keywords:	geometrically nonlinear mechanical systems, structure preserving discretization, non-uniform boundary conditions, weak form, port-Hamiltonian systems, mixed finite elements, continuums mechanics, mechanical systems
Note: The following files were submitted by the author for peer review, but cannot be converted to PDF. You must view these files (e.g. movies) online.	
ThomKoty_MCMDS_2022.tex	

ARTICLE

Explicit port-Hamiltonian FEM models for geometrically nonlinear mechanical systems

Tobias Thoma[a] and Paul Kotyczka[a]

[a]T. Thoma & P. Kotyczka, Technical University of Munich, TUM School of Engineering and Design, Chair of Automatic Control, Garching, Germany

ARTICLE HISTORY
Compiled February 4, 2022

ABSTRACT
In this article, we present the port-Hamiltonian representation, the structure preserving discretization and the resulting finite-dimensional state space model of geometrically nonlinear mechanical systems based on a mixed finite element formulation. This article focuses on St. Venant–Kirchhoff materials connecting the Green strain and the second Piola-Kirchhoff stress tensor in a linear relationship which allows a port-Hamiltonian representation by means of its co-energy (effort) variables. Due to treatment of both Dirichlet and Neumann boundary conditions in the appropriate variational formulation, the resulting port-Hamiltonian state space model features both of them as explicit (control) inputs. Numerical experiments generated with FEniCS illustrate the properties of the resulting FE models.

KEYWORDS
port-Hamiltonian systems; mixed finite elements; geometrically nonlinear mechanical systems; structure preserving discretization; non-uniform boundary conditions; weak form

1. Introduction

Port-Hamiltonian (PH) systems provide a framework for modeling, analysis and control of complex dynamical systems [1] where the complexity might result from multi-physical couplings, non-trivial domains and nonlinearity. Since several engineering problems are described by partial differential equations (PDEs), the theory of infinite dimensional port-Hamiltonian [2, 3] systems has become increasingly important in recent years and a great progress has been achieved in modeling different physical domains by means of the PH framework [4]. Also the possibilities and advantages of the PH formulation for structural mechanics have already been shown in several articles, e.g. [5, 6].

While a lot effort has already been put into the development of PH systems for linear solid mechanics [7–10], the nonlinear cases were handled rarely. Nonlinear effects – like for example large deformations – in the modeling of port-Hamiltonian systems in the field of structural mechanics have already been discussed in some articles. A suitable method to display the nonlinear effect due to large rotations of flexible structures is the coupling of a nonlinear rigid body system with the partial differential

CONTACT T. Thoma. Email: tobias.thoma@tum.de

equations of linear elastodynamics [5, 11]. However, this approach is not compatible with large distortions. In order to gain a more accurate model, the nonlinear PDEs of solid mechanics have to be considered. In the current literature there are contributions dealing with port-Hamiltonian modeling and structure-preserving discretization [12] of nonlinear beams [13] and plates [14]. To the best of our knowledge, a general consideration of arbitrary geometrically nonlinear[1] continua is not present in the current literature.

In this contribution, we focus on the mixed finite element formulation of geometrically nonlinear mechanical systems where both Dirichlet and Neumann boundary conditions are applied in a weak sense [15, 16]. Due to the fact that only geometrically nonlinear systems are considered, their PH representation can be expressed in terms of their effort variables with a quadratic Hamiltonian. The nonlinear effect is apparent in the resulting in/-output and energy shifting matrix. A similar state space structure of the finite dimensional system can be found in [13] and [14] where also only geometrically nonlinearity of beams and shells (special one/two-dimensional continua) are treated. In this article, PH modeling of general three-dimensional geometrically nonlinear continua is treated, where, unlike in [13], Lagrange multipliers can additionally be omitted to satisfy different boundary conditions.

This article is organized as follows. In Section 2 we recall the basics of nonlinear continuum mechanics and show a PH representation for geometrically nonlinear, three-dimensional mechanical systems. The mixed finite element discretization procedure with weakly imposed boundary ports is demonstrated in Section 3. Section 4 focuses on numerical simulations and their discussion and Section 5 gives a short conclusion.

2. Modeling

This sections recalls the governing equations of nonlinear continuum mechanics for St. Venant–Kirchhoff materials and presents their PH representation.

2.1. Nonlinear continuum mechanics

In the following, we subdivide the theory of nonlinear continuum mechanics [17] into three components, kinematics, balance equations (dynamics) and constitutive equations (material laws).

2.1.1. Kinematics

In this article we consider a Boltzmann continuum[2] Ω embedded in the three dimensional Euclidean space $\mathbb{R}^3$ and consisting of a continuous set of points or particles $x \in \Omega$. The deformation of a body Ω_t at time t is fully described by the spatial position $x(X,t)$ of each material point X of the initial (undeformed) configuration $\Omega_0 \subset \mathbb{R}^3$ at $t = t_0$. Therefore, we get the *displacement field*

$$u(X,t) = x(X,t) - x(X,t_0) = x(X,t) - X \tag{1}$$

of a body $\forall t \in [t_0, t_e]$.

[1]Due to the strong geometry change of a body, the basic mechanical equations have to be represented by nonlinear functions.

[2]Infinitesimal volume elements do not contain rotational inertia.

One of the most important quantities in nonlinear continuum mechanics is the so-called *deformation gradient*

$$F(X,t) = \frac{\partial x(X,t)}{\partial X} = \frac{\partial u(X,t)}{\partial X} + I, \tag{2}$$

where $I \in \mathbb{R}^{3\times 3}$ represents the second order identity tensor[3]. The deformation gradient maps the infinitesimal material line element dX of the initial configuration to the spatial fiber dx of the deformed one,

$$dx = F \cdot dX. \tag{3}$$

This process is clarified in Fig. 1. The concept of deformation gradient allows to transfer different mechanical quantities, e.g. stresses, from the material configuration Ω_0 to the spatial one Ω_t, and vice-versa.

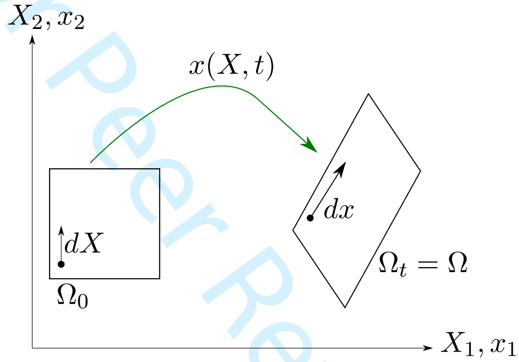

Figure 1. Mapping of a infinitesimal fiber from the initial (undeformed) configuration to the current (deformed) one ($\Omega \subset \mathbb{R}^2$).

In order to define a suitable *strain measure* based on the material configuration, it must contain *material objectivity* and thus be independent of rigid body deformations. Since $F^T \cdot F - I = 0$ for arbitrary pure rigid body deformations [18], the *symmetric Green strain tensor*

$$E(X,t) = \frac{1}{2}(F^T(X,t) \cdot F(X,t) - I) \tag{4}$$

represents one of the simplest *nonlinear strain measures*.

Remark 1. In case of small deformations the Green strain tensor can be approximated (linearized) by

$$\epsilon = \lim_{\|\frac{\partial u}{\partial X}\| \to 0} E(u,t) = \frac{1}{2}\left[\left(\frac{\partial u}{\partial X}\right)^T + \left(\frac{\partial u}{\partial X}\right)\right], \tag{5}$$

where ϵ represents the well-known strain measure of linear elastodynamics [19]. It is important to notice that this strain measure is only valid for small deformations.

[3]I.e., the identity matrix

Notation 1. From now on, we mainly focus on characteristics of the material configuration, where all field quantities depend on the spatial coordinate X and the time t, which we omit for brevity.

2.1.2. Balance equations

An essential property of balance equations is the option to demonstrate them equivalently in six different forms by using material or spatial quantities globally for an entire body, locally at a point or in a stationary control volume of the body. Since we focus on structural mechanics (and finite element discretization in the next section), we only recall major balance equations locally in material coordinates.

At first we start with the local translational equilibrium

$$\rho_0 \ddot{u} = \mathrm{Div}(F \cdot S) + f_0 \tag{6}$$

represented in the material coordinate system. This balance equation describes the linear momentum of an infinitesimal volume element related to the initial configuration. It contains the density $\rho_0 \in \mathbb{R}$ of Ω_0, the acceleration field

$$\ddot{u} = \frac{\partial}{\partial t}\left(\frac{\partial u}{\partial t}\right) = \frac{\partial v}{\partial t} = \dot{v}, \tag{7}$$

the deformation gradient F, the *symmetric second Piola–Kirchhoff stress tensor*[4] $S \in \mathbb{R}^{3\times 3}$ and the volume forces $f_0 \in \mathbb{R}^3$.

Notation 2. The operator

$$\mathrm{Div}(\times) = \frac{\partial(\times)}{\partial X} : I \tag{8}$$

represents the divergence and

$$\mathrm{Grad}(\times) = \frac{\partial(\times)}{\partial X} \tag{9}$$

the gradient of a tensor with respect to the material coordinate system. For more information the reader is referred to Appendix A.

Assumption 1. For simplicity, we assume that no forces per unit undeformed volume, e.g. gravity, are present, accordingly $f_0 = 0$. This is not a major restriction, since in the case of a PH representation these forces can be completed by adding an external port.

Since the sum of all moments with respect to any point vanishes, the rotational equilibrium is automatically fulfilled due to the symmetry of the Cauchy stress tensor[5] and accordingly $S = S^T$. The mass balance follows by the fact that $\dot{\rho}_0 = 0$. Therefore both relationships can be accommodated in (6). Since the (pure mechanical) energy

[4]The second Piola–Kirchhoff stresses are related to the symmetric Cauchy stresses $\sigma = \sigma^T$ via $S = \det(F)F^{-1}\sigma F^{-T}$.

[5]The symmetry of the Cauchy tensor is only valid for a Boltzmann continuum, because in this case no rotational inertia is assigned to the infinitesimal volume elements.

balance directly results from (6), it does not need to be explicitly stated for solving an initial boundary value problem.

2.1.3. Constitutive equations

In order to achieve a full description of nonlinear continua, constitutive equations or material laws are required. In terms of elastic solids they provide a relation between stress and strain. According to this relation, the *stored strain energy function* or *elastic potential* per unit undeformed volume can be defined.

Assumption 2. In this article we only consider pure mechanical isothermal behavior. Therefore, the internal energy of the continuum corresponds to the elastic potential. This fact will become more relevant, when it comes to the port-Hamiltonian representation.

Deformations in *hyperelastic* materials are completely reversible and characterized by a stored strain energy function Ψ. The *St. Venant–Kirchhoff material* represents a special hyperelastic material with a linear relation between the second Piola–Kirchhoff stresses and the geometrically nonlinear Green strains. This relation is given by

$$S = C : E \tag{10}$$

and leads to

$$\Psi(E) = \frac{1}{2} E : C : E \tag{11}$$

including the constant symmetric fourth order tensor $C \in \mathbb{R}^{3\times3\times3\times3}$, known as the *Lagrangian* or material elasticity tensor. It includes two second order identity tensors I, the symmetric forth order identity tensor $\mathcal{I}_s$ and Lamé's coefficients μ and λ,

$$C = 2\mu\mathcal{I}_s + \lambda I \otimes I. \tag{12}$$

Remark 2. The St. Venant–Kirchhoff material represents a geometrically nonlinear generalization of Hooke's law. Both material laws share the same elasticity tensor C, which, however, relates different stresses and strains. Due to material objectivity of the strain tensor E, St. Venant–Kirchhoff materials can handle large displacements and rotations but are only valid for moderate distortions.

2.2. Port-Hamiltonian model

In this section, we represent a port-Hamiltonian formulation of geometrically nonlinear mechanical systems. We consider linear St. Venant–Kirchhoff materials and nonlinear kinematics set by Green strains.

2.2.1. State differential equations

Due to the assumption of geometrical nonlinearity, the total energy

$$H = \frac{1}{2} \int_{\Omega_0} p \cdot p \frac{1}{\rho_0} + E : C : E \, d\Omega_0. \tag{13}$$

can be rewritten in terms of the linear momenta $p = \rho_0 v \in \mathbb{R}^3$ and the symmetric Green strain tensor $E \in \mathbb{R}^{3\times 3}$ as energy variables (states). By applying the variational derivatives, which, for the Hamiltonian without spatial derivatives, are simply the partial derivatives of the Hamiltonian density,

$$\frac{\delta H(p,E)}{\delta p} = \dot{u} \tag{14}$$

$$\frac{\delta H(p,E)}{\delta E} = C : E, \tag{15}$$

we obtain as co-energy variables (efforts) the velocities $v \in \mathbb{R}^3$ and stresses $S \in \mathbb{R}^{3\times 3}$.

Theorem 2.1. *The state differential equations in PH form representing geometrically nonlinear St. Venant–Kirchhoff materials are given by*

$$\begin{bmatrix} \dot{p} \\ \dot{E} \\ \dot{F} \end{bmatrix} = \mathcal{J}(F) \begin{bmatrix} \frac{\delta H}{\delta p} \\ \frac{\delta H}{\delta E} \\ \frac{\delta H}{\delta F} \end{bmatrix} \tag{16}$$

with the quadratic Hamiltonian (13) *and the formally skew-adjoint operator*

$$\mathcal{J}(F) = \begin{bmatrix} 0 & \mathrm{Div}(F \cdot \times) & \mathrm{Div}(\times) \\ a(F,\times) & 0 & 0 \\ \mathrm{Grad}(\times) & 0 & 0 \end{bmatrix} \tag{17}$$

in which

$$a(F,\times) = \frac{1}{2}\left(F^T \cdot \mathrm{Grad}(\times) + \mathrm{Grad}(\times)^T \cdot F\right). \tag{18}$$

Proof. In order to get the first state equation of the PH form (16), the left hand side of (6) is rewritten by means of the linear momenta p. Taking the deformation gradient rate

$$\dot{F} = \mathrm{Grad}(v) \tag{19}$$

and inserting it into the time derivative of the Green strain tensor

$$\dot{E} = \frac{1}{2}\left(F^T \cdot \dot{F} + \dot{F}^T \cdot F\right) \tag{20}$$

leads to the second state equation. In order to close the system, an extra equation for F has to be included what leads to the augmented system (16). The formal skew-adjointness of the operator $\mathcal{J}(F)$ becomes more obvious by writing (16) in its vector notation, where the symmetry of E and S are taken into account. For more information we refer to Appendix B. □

Since we assume that $H(p,E)$ does not explicitly depend on F, it follows $T = \frac{\delta H}{\delta F} = 0$. Due to the choice of state variables, the port-Hamiltonian representation (16) can be rewritten in terms of acceleration and stress rate,

$$\begin{bmatrix} \rho_0 \dot{v} \\ C^{-1} : \dot{S} \\ \dot{F} \end{bmatrix} = \mathcal{J}(F) \begin{bmatrix} v \\ S \\ 0 \end{bmatrix}. \tag{21}$$

Remark 3. If the elastic potential $\Psi(E, F)$ depends also on the deformation gradient F, it follows

$$T = \frac{\delta H}{\delta F} \neq 0 \in \mathbb{R}^{3\times 3}, \tag{22}$$

where T has the character of a first Piola–Kirchhoff stress tensor, what could already be guessed from (16). Since $\mathcal{J}(F)$ connects T and $\dot{p}$ via the divergence operator, only first Piola-Kirchhoff stresses are compatible with the local translational equilibrium. The case $T \neq 0$ might lead to a materially nonlinear behavior, what we do not consider in this article.

2.2.2. Energy balance and boundary ports

The formal skew-adjointness of the operator $\mathcal{J}(F)$ implies the energy balance

$$\begin{aligned} \dot{H} &= \int_{\Omega_0} \frac{\delta H}{\delta p} \cdot \dot{p} + \frac{\delta H}{\delta E} : \dot{E} + \frac{\delta H}{\delta F} : \dot{F} \, d\Omega_0 \\ &= \int_{\partial\Omega_0} v \cdot F \cdot S \cdot N \, d\partial\Omega_0, \end{aligned} \tag{23}$$

where the state differential equations are inserted and integration by parts is applied to one of the addends (see Appendix C). $N \in \mathbb{R}^3$ represents the outer normal vector in the boundary $\partial\Omega_0$.

Besides the strong form (21), the initial and boundary conditions form the initial boundary value problem of the PH system. Since this article focuses on the representation of a PH FEM model with *non-uniform* boundary conditions, the boundary $\partial\Omega_0 = \Sigma_D \cup \Sigma_N$ is split into two (passivity disjoint) subsets on which the Neumann and Dirichlet boundary conditions are applied. The Neumann condition

$$F \cdot S \cdot N = \bar{\tau}_0 \qquad \text{on} \quad \Sigma_N \tag{24}$$

with the traction vector per unit initial area $\bar{\tau}_0 \in \mathbb{R}^3$ results form the infinitesimal equilibrium at the surface based on the material coordinate system. The Dirichlet condition

$$v = \bar{\nu} \qquad \text{on} \quad \Sigma_D \tag{25}$$

imposes the desired velocity $\bar{\nu} \in \mathbb{R}^3$ on the surface. Declaring the boundary inputs $u_N = \bar{\tau}_0$ on Σ_N and $u_D = \nu$ on Σ_D according to (24) and (25), we can define the collocated and power-conjugated outputs $y_N = v$ on Σ_N and $y_D = F \cdot S \cdot N$ on Σ_D. The continuous power balance

$$\dot{H} = \int_{\Sigma_N} u_N \cdot y_N \, d\Sigma_N + \int_{\Sigma_D} u_D \cdot y_D \, d\Sigma_D \tag{26}$$

shows the power introduced via the boundary $\partial\Omega_0$.

3. Mixed FE formulation

In this section, we derive the finite dimensional PH representation of a geometrically nonlinear mechanical system based on the mixed finite element method [20]. The resulting ordinary differential equations represent a nonlinear port-Hamiltonian system with a quadratic Hamiltonian.

3.1. Weak form

To derive a finite element discretization, a weak (or variational) form of (16) or (21) is required. Due to the symmetry of δS (see Appendix D) the weak form of (21) is given by

$$\begin{aligned}\delta P_v = \int_{\Omega_0} \delta v \cdot \rho_0 \dot{v} - \delta v \cdot \mathrm{Div}(F \cdot S)\, d\Omega_0 \\ + \int_{\Sigma_N} \delta v \cdot (F \cdot S \cdot N - \bar{\tau}_0)\, d\Sigma_N = 0\end{aligned} \tag{27a}$$

$$\begin{aligned}\delta P_S = \int_{\Omega_0} \delta S : C^{-1} : \dot{S} - \delta S : \left(F^T \cdot \mathrm{Grad}(v)\right)\, d\Omega_0 \\ + \int_{\Sigma_D} F \cdot \delta S \cdot N \cdot (v - \bar{\nu})\, d\Sigma_D = 0\end{aligned} \tag{27b}$$

$$\delta P_T = \int_{\Omega_0} \delta T : \dot{F} - \delta T : \mathrm{Grad}(v)\, d\Omega_0 = 0 \tag{27c}$$

for all test functions δv, δS and δT. Due to the choice of test functions the weak form can be interpreted in terms of virtual power. In case of (27a) the principle of virtual velocities fulfills the force equilibrium and the principle of virtual forces/stresses in (27b) and (27c) the kinematics. Compared to the standard approach of the *partitioned finite element method* [12], both the Neumann and Dirichlet boundary conditions are already introduced in the weak form through the boundary terms in (27a) and (27b) which amount for zero if the boundary conditions are satisfied. See [16] for the case of linear mechanical systems.

Notation 3. So far, all equations have been expressed using tensors. However, in the finite element method, a vector notation is usually used. In the following, the corresponding vector or matrix representation of a tensor is indicated by means of underscores.

3.2. Discretization

Theorem 3.1. *By applying a mixed Galerkin discretization of* (21) *with Neumann and Dirichlet boundary conditions* (24) *and* (25) *based on the weak formulation* (27) *and using trial and test functions from the same bases*

$$\begin{aligned} v(X,t) &= \phi(X)\cdot\hat{v}(t), & \delta v(X) &= \phi(X)\cdot\delta\hat{v},\\ S(X,t) &= \psi(X)\cdot\hat{S}(t), & \delta v(X) &= \psi(X)\cdot\delta\hat{S},\\ F(X,t) &= \theta(X)\cdot\hat{F}(t), & \delta T(X) &= \theta(X)\cdot\delta\hat{T},\\ \bar{\tau}_0(X,t) &= \xi(X)\cdot\hat{\tau}_0(t), & \bar{\nu}(X,t) &= \zeta(X)\cdot\hat{\nu}(t), \end{aligned}$$

the PH state space model

$$\begin{aligned} \underbrace{\begin{bmatrix} \underline{M}_v & 0 & 0\\ 0 & \underline{M}_S & 0\\ 0 & 0 & \underline{M}_F \end{bmatrix}}_{\underline{M}=\underline{M}^T>0} \begin{bmatrix} \dot{\hat{\underline{v}}}\\ \dot{\hat{\underline{S}}}\\ \dot{\hat{\underline{F}}} \end{bmatrix} &= \underbrace{\begin{bmatrix} 0 & -\underline{K}(\hat{\underline{F}}) & -\underline{Z}^T\\ \underline{K}^T(\hat{\underline{F}}) & 0 & 0\\ \underline{Z} & 0 & 0 \end{bmatrix}}_{\underline{J}=-\underline{J}^T} \begin{bmatrix} \hat{\underline{v}}\\ \hat{\underline{S}}\\ 0 \end{bmatrix}\\ &\quad + \underbrace{\begin{bmatrix} \underline{G}_\tau & 0\\ 0 & \underline{G}_\nu(\hat{\underline{F}})\\ 0 & 0 \end{bmatrix}}_{\underline{G}} \begin{bmatrix} \hat{\underline{\tau}}_0\\ \hat{\underline{\nu}} \end{bmatrix} \end{aligned} \tag{28}$$

$$\underline{y} = \underbrace{\begin{bmatrix} \underline{G}_\tau^T & 0 & 0\\ 0 & \underline{G}_\nu^T(\hat{\underline{F}}) & 0 \end{bmatrix}}_{\underline{G}^T} \begin{bmatrix} \hat{\underline{v}}\\ \hat{\underline{S}}\\ 0 \end{bmatrix} \tag{29}$$

with the approximate quadratic Hamiltonian

$$\hat{H} = \frac{1}{2}\hat{\underline{v}}^T\underline{M}_v\hat{\underline{v}} + \frac{1}{2}\hat{\underline{S}}^T\underline{M}_S\hat{\underline{S}} \tag{30}$$

is obtained. The expressions of the matrices are given in Appendix E.

Proof. Integration by parts of (27a) leads to

$$\begin{aligned} \delta P_v = \int_{\Omega_0} & \delta v\cdot\rho_0\dot{v} + (\mathrm{Grad}(\delta v)^T\cdot F) : S\; d\Omega_0\\ & - \int_{\partial\Omega_0} \delta v\cdot F\cdot S\cdot N\; d\partial\Omega_0\\ & + \int_{\Sigma_N} \delta v\cdot(F\cdot S\cdot N - \bar{\tau}_0)\; d\Sigma_N = 0 \end{aligned} \tag{31}$$

Since the boundary $\partial\Omega_0$ can be split in a Neumann and Dirichlet part, we achieve

$$\begin{aligned}\delta P_v = \int_{\Omega_0} \delta v \cdot \rho_0 \dot{v} + (\mathrm{Grad}(\delta v)^T \cdot F) : S \, d\Omega_0 \\ - \int_{\Sigma_D} \delta v \cdot F \cdot S \cdot N \, d\Sigma_D \\ - \int_{\Sigma_N} \delta v \cdot \bar{\tau}_0 \, d\Sigma_N = 0\end{aligned} \tag{32a}$$

$$\begin{aligned}\delta P_S = \int_{\Omega_0} \delta S : C^{-1} : \dot{S} - \delta S : \left(F^T \cdot \mathrm{Grad}(v)\right) \, d\Omega_0 \\ + \int_{\Sigma_D} F \cdot \delta S \cdot N \cdot v \, d\Sigma_D \\ - \int_{\Sigma_D} F \cdot \delta S \cdot N \cdot \bar{\nu} \, d\Sigma_D = 0\end{aligned} \tag{32b}$$

$$\delta P_T = \int_{\Omega_0} \delta T : \dot{F} - \delta T : \mathrm{Grad}(v) \, d\Omega_0 = 0. \tag{32c}$$

Rearranging the weak form (32) in its vector notation (see Appendix E) leads to

$$\begin{aligned}\delta P_v = \int_{\Omega_0} \underline{\delta v}^T \rho_0 \underline{\dot{v}} + (\underline{D}\, \underline{\delta v})^T \underline{F}\, \underline{S} \, d\Omega_0 \\ - \int_{\Sigma_D} \underline{\delta v}^T \underline{N}\, \underline{F}\, \underline{S} \, d\Sigma_D \\ - \int_{\Sigma_N} \underline{\delta v}^T \underline{\bar{\tau}}_0 \, d\Sigma_N = 0\end{aligned} \tag{33a}$$

$$\begin{aligned}\delta P_S = \int_{\Omega_0} \underline{\delta S}^T \underline{C}^{-1} \underline{\dot{S}} - \underline{\delta S}^T \underline{F}^T (\underline{D}\, \underline{v}) \, d\Omega_0 \\ + \int_{\Sigma_D} \underline{\delta S}^T \underline{F}^T \underline{N}^T \underline{v} \, d\Sigma_D \\ - \int_{\Sigma_D} \underline{\delta S}^T \underline{F}^T \underline{N}^T \underline{\bar{\nu}} \, d\Sigma_D = 0\end{aligned} \tag{33b}$$

$$\delta P_T = \int_{\Omega_0} \underline{\delta T}^T \underline{\dot{F}} - \underline{\delta T}^T (\underline{D}\, \underline{v}) \, d\Omega_0 = 0 \tag{33c}$$

containing the differential operator $\underline{D}$ representing the gradient. Inserting the approximations depending on the basis functions in vector notation allows us to take all variables except $\underline{\hat{F}}$ out of the integrals. Since $\delta\hat{S}$, $\delta\hat{v}$ and $\delta\hat{T}$ are arbitrary we get (28). The discrete Hamiltonian (30) is obtained by substituting the approximated co-energy variables into $H(v, S)$. Its time derivative

$$\dot{\hat{H}} = \underline{\hat{v}}^T \underline{G}_\tau \underline{\hat{\tau}}_0 + \underline{\hat{S}}^T \underline{G}_\nu (\underline{\hat{F}}) \underline{\hat{\nu}} \tag{34}$$

gives the power conjugated output (29), which concludes the proof. □

Remark 4. Since the models of [13] and [14] are (due to further assumptions) a special case of the theory recalled in this article, the similarity of the resulting PH FEM models is no surprise.

4. Numerical results

The performance of our approach is now demonstrated with simple FEniCS [21] simulations.

4.1. One-dimensional rod

We consider the geometrically nonlinear one-dimensional rod, a linear version of this has been treated in [16], except that only non-homogeneous boundary conditions are considered here. The one-dimensional rod

$$\rho_0 \cdot \dot{v} = \frac{\partial (F \cdot S)}{\partial X} \tag{35a}$$

$$\frac{\dot{S}}{EA} = F \cdot \frac{\partial v}{\partial X} \tag{35b}$$

$$\dot{F} = \frac{\partial v}{\partial X} \tag{35c}$$

with length L is our first benchmark system. It includes the boundary

$$v(X = 0, t) = \bar{\nu} \tag{36}$$

$$F(X = L, t) \cdot S(X = L, t) = \bar{\tau}_0 \tag{37}$$

and initial conditions

$$v(X, t = 0) = 0.5 \text{ m/s} \tag{38}$$

$$S(X, t = 0) = 0 \text{ N} \tag{39}$$

$$F(X, t = 0) = 1. \tag{40}$$

The rod is first discretized with 100 and then 200 equidistant elements, second order Lagrange polynomials for ϕ, second order discontinuous basis functions for ψ - due to the third equation in (21) - and first order discontinuous basis functions for θ - due to (4) and (15).

The system is simulated for $T = 1$ s using the implicit midpoint rule and sampling time 1 ms where the nonlinear equations are solved using Newton iterations. Further simulation parameters are listed in Table 1.

Figure 2 shows the Hamiltonian which keeps its constant level for $t \geq 0.2$ s due to the fact that no more power is transmitted at the boundaries. Figure 3 and 4 demonstrate the behavior of Dirichlet and Neumann conditions which are introduced in a weak sense. For the sake of completeness, the velocity $v(X = L, t)$ is illustrated in Figure 5.

Table 1. Simulation parameters of the rod

Symbol	Value
L	3 m
ρ_0	7.850 kg/m
E	$1000\,\mathrm{N/mm^2}$
A	$100\,\mathrm{mm^2}$
$\bar{\nu}$	$\begin{cases}(1-\frac{t}{0.2\text{ s}})\cdot 0.5\text{ m/s} & \forall t\leq 0.2\text{ s}\\ 0\text{ m/s} & \forall t>0.2\text{ s}\end{cases}$
$\bar{\tau}_0$	$\begin{cases}100\text{ N} & \forall t\leq 0.2\text{ s}\\ 0\text{ N} & \forall t>0.2\text{ s}\end{cases}$

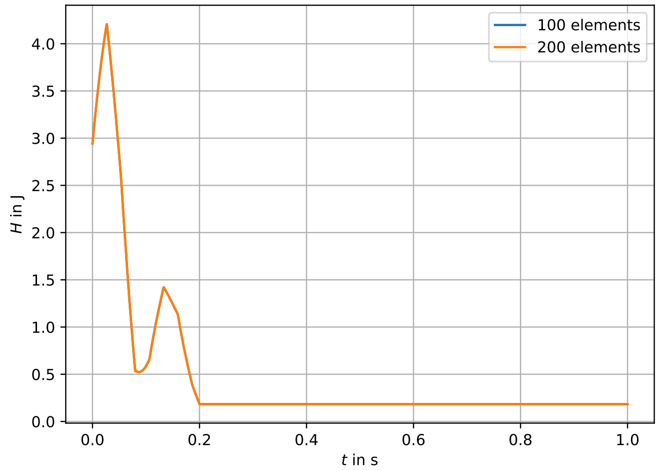

Figure 2. Total energy H of the rod

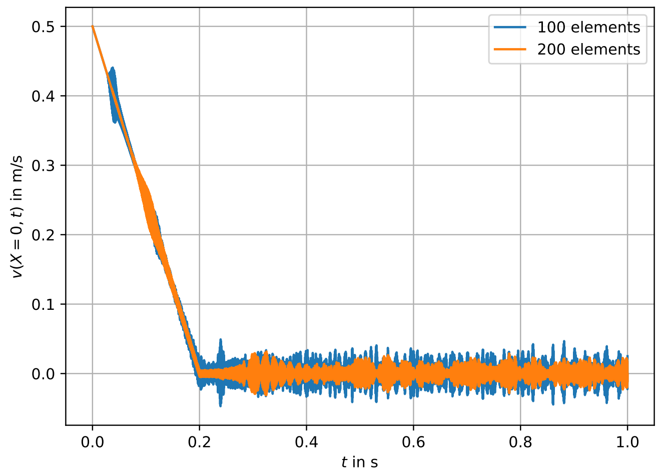

Figure 3. Rod velocity $v(X=0,t)$ meets $\bar{\nu}$ in a week sense

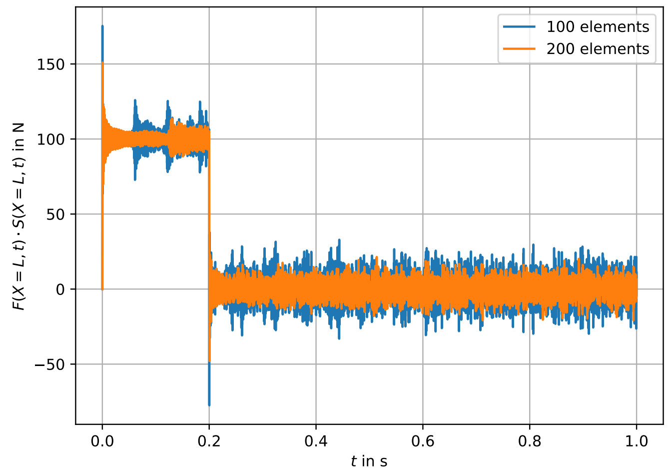

Figure 4. Rod normal force $F(X = L, t) \cdot S(X = L, t)$ meets $\bar{\tau}_0$ in a week sense

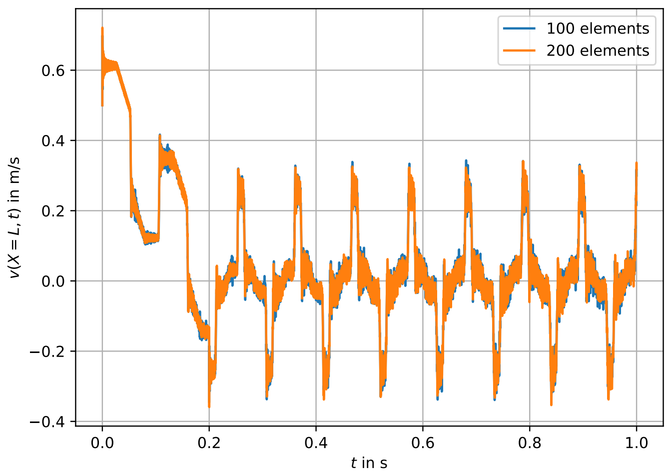

Figure 5. Rod velocity $v(X = L, t)$

4.2. Two-dimensional beam

This section focuses on the simulation of a geometrically nonlinear two-dimensional beam in plane stress, see Figure 6. It contains unit thickness ($L_z = 1$ m) and is subject to the boundary

$$v(X_1 = 0, X_2, t) = \bar{\nu}(t) \tag{41}$$
$$F(X_1, X_2 = 0, t) \cdot S(X_1, X_2 = 0, t) \cdot N = 0 \tag{42}$$
$$F(X_1 = L_x, X_2, t) \cdot S(X_1 = L_x, X_2, t) \cdot N = \tau_{L_x}(t) \tag{43}$$
$$F(X_1, X_2 = L_y, t) \cdot S(X_1, X_2 = L_y, t) \cdot N = 0 \tag{44}$$

and initial conditions

$$v(X, t = 0) = 0 \text{ m/s} \tag{45}$$
$$S(X, t = 0) = 0 \text{ N} \tag{46}$$
$$F(X, t = 0) = I. \tag{47}$$

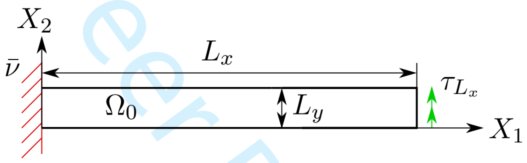

Figure 6. Two-dimensional beam. The beam of length L_x and height L_y is firmly clamped on its left side and is gripped by the load τ_{L_x} on its right side. The figure shows the initial configuration, where $u(X, t = t_0) = 0$ m.

The beam is discretized with 1250 equidistant triangle elements, first order Lagrange polynomials for ϕ (velocities), first order discontinuous basis functions for ψ (second Piola–Kirchhoff stresses) and zero order discontinuous basis functions for θ (deformation gradient). Since the boundary conditions τ_{L_x} and $\bar{\nu}$ do not explicitly depend on the spatial coordinate X (see Table 2), ξ and ζ are not required.

The beam system is simulated for $T = 4$ s using the implicit midpoint rule and sampling time 1 ms where the nonlinear equations are again solved by Newton iterations. Further simulation parameters are demonstrated in Table 2.

Table 2. Simulation parameters of the beam

Symbol	Value
L_x	25 m
L_y	1 m
ρ_0	$1.02 \cdot 10^{-4}$ kg/m^3
λ	329.67 N/m^2
μ	384.62 N/m^2
$\bar{\nu}$	$\begin{bmatrix} 0 \text{ m/s} & 0 \text{ m/s} \end{bmatrix}^T$
τ_{L_x}	$\begin{cases} \begin{bmatrix} 0 \text{ N/m}^2 & \frac{t}{1\text{s}} \cdot 0.1 \text{ N/m}^2 \end{bmatrix}^T & \forall t \leq 1 \text{ s} \\ \begin{bmatrix} 0 \text{ N/m}^2 & 0 \text{ N/m}^2 \end{bmatrix}^T & \forall t > 1 \text{ s} \end{cases}$

Remark 5. To illustrate the need for a nonlinear simulation for this example system, we set up the initial boundary value problem with the assumptions of linear elastodynamics for comparison. These linear partial differential equations are solved with the

same mesh as described above. Furthermore, the velocity field is also approximated with first order Lagrange polynomials. For more information on the PH finite element modeling of linear elastodynamics we refer to [16].

The Hamiltonian of the geometrically nonlinear PH beam model and the linear one is shown in Figure 7. Both graphs show the expected constant behavior at $t \geq 1$ s.

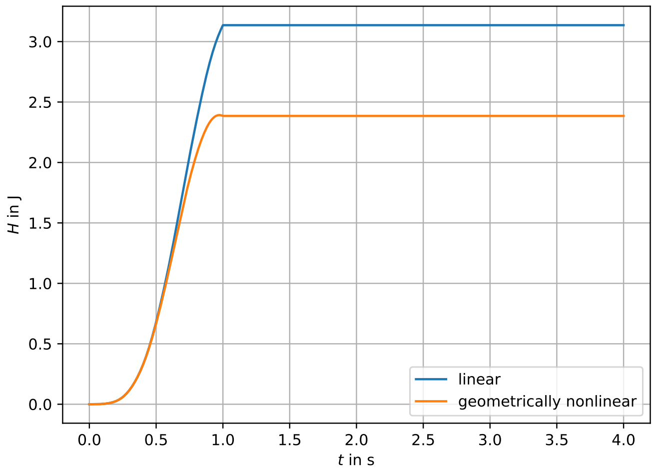

Figure 7. Total energy H of the beam. The orange line represents the Hamiltonian of the geometrically nonlinear beam. The blue line shows the Hamiltonian of the linear beam model, which is significantly higher than that of the nonlinear one. This unphysical behavior results from the linear modeling or the linear strain measure (see Remark 1). This has no material objectivity and thus adds energy to the system during rotations.

In order to get the displacements u, see Figure 8, the velocity field v is integrated using the implicit midpoint rule as described above. Using ParaView [22] the entire displacement field can be easily visualized, see Figure 9.

5. Conclusions

We presented a mixed finite element discretization procedure for a special class of nonlinear mechanical systems in order to achieve a PH state space model. The considered system class is based on St. Venant–Kirchhoff materials connecting the Green strain and second Piola-Kirchhoff stress tensor in a linear relationship. Due to the chosen structure of the weak form and an appropriate discretization, a PH state space model could be generated which considers as explicit inputs both the Dirichlet and Neumann boundary conditions.

Even though St. Venant–Kirchhoff materials are a commonly used tool, they are not suitable for considering more complex material processes, e.g. biological tissue. Accordingly, we are currently working on the PH representation of more complex solid mechanical systems and the associated structure-preserving discretization procedures.

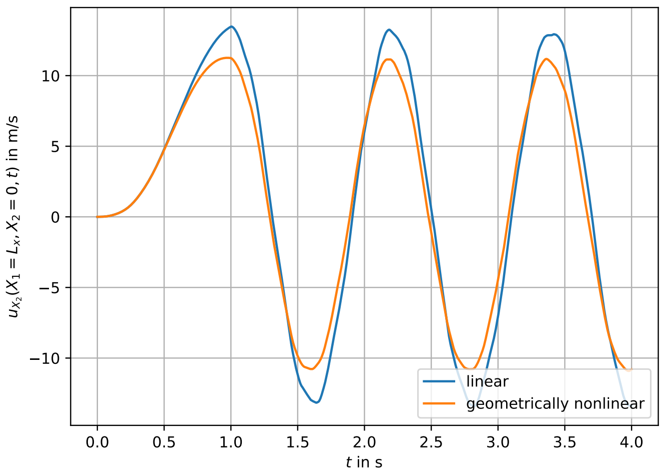

Figure 8. Beam displacement $u_{X_2}(X_1 = L_x, X_2 = 0, t)$. The graphs show the displacement in X_2-direction of a special mesh node. Compared to the geometrically nonlinear beam, the linear one generally shows a higher displacement. The reason for this becomes clear in Figure 9.

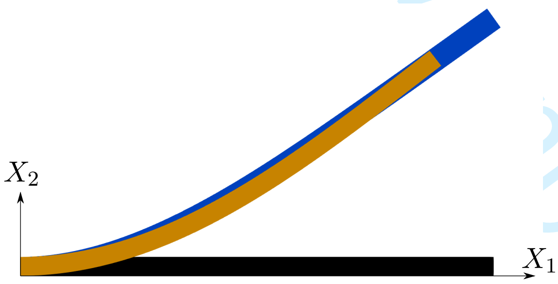

Figure 9. Beam displacement field $u(X, t = 2.2\text{ s})$. The orange beam display represents the displacement field of the geometrically nonlinear simulation at $t = 2.2$ s. The blue one represents the displacement field of the linear simulation at $t = 2.2$ s and the black one shows the initial configuration. It can be seen that the volume of the linear beam shows a significant increase compared to volume of the nonlinear one. This unrealistic effect, which is also evident in Figure 7, is due to the linear strain measure.

Acknowledgments

The authors thank Boris Lohmann, Tim Moser and Christopher Lerch for fruitful discussions.

References

[1] V. Duindam, A. Macchelli, S. Stramigioli, and H. Bruyninckx, *Modeling and Control of Complex Physical Systems*, Springer Berlin Heidelberg, 2009.
[2] B. Jacob and H. Zwart, *Linear Port-Hamiltonian Systems on Infinite-dimensional Spaces*, Vol. 223, Springer, 2012.
[3] P. Kotyczka, *Numerical Methods for Distributed Parameter Port-Hamiltonian Systems*, TUM.University Press, 2019.
[4] R. Rashad, F. Califano, A.J. van der Schaft, and S. Stramigioli, *Twenty years of distributed port-Hamiltonian systems: A literature review*, IMA Journal of Mathematical Control and Information 37 (2020), pp. 1400–1422.
[5] A. Brugnoli, D. Alazard, V. Pommier-Budinger, and D. Matignon, *Port-Hamiltonian flexible multibody dynamics*, Multibody System Dynamics 51 (2020), pp. 343–375.
[6] A. Warsewa, M. Böhm, O. Sawodny, and C. Tarín, *A port-Hamiltonian approach to modeling the structural dynamics of complex systems*, Applied Mathematical Modelling 89 (2021), pp. 1528–1546.
[7] A. Macchelli and C. Melchiorri, *Modeling and control of the Timoshenko beam. The distributed port-Hamiltonian approach*, SIAM Journal on Control and Optimization 43 (2004), pp. 743–767.
[8] S. Aoues, F.L. Cardoso-Ribeiro, D. Matignon, and D. Alazard, *Modeling and control of a rotating flexible spacecraft: A port-Hamiltonian approach*, IEEE Transactions on Control Systems Technology 27 (2019), pp. 355–362.
[9] A. Brugnoli, D. Alazard, V. Pommier-Budinger, and D. Matignon, *Port-Hamiltonian formulation and symplectic discretization of plate models part I: Mindlin model for thick plates* (2019).
[10] A. Brugnoli, D. Alazard, V. Pommier-Budinger, and D. Matignon, *Port-Hamiltonian formulation and symplectic discretization of plate models part II: Kirchhoff model for thin plates* (2019).
[11] A. Macchelli, C. Melchiorri, and S. Stramigioli, *Port-based modeling and simulation of mechanical systems with rigid and flexible links*, IEEE Transactions on Robotics 25 (2009), pp. 1016–1029.
[12] F.L. Cardoso-Ribeiro, D. Matignon, and L. Lefèvre, *A partitioned finite element method for power-preserving discretization of open systems of conservation laws*, IMA Journal of Mathematical Control and Information (2020).
[13] A. Brugnoli, R. Rashad, F. Califano, S. Stramigioli, and D. Matignon, *Mixed finite elements for port-Hamiltonian models of von-Kármán beams*, IFAC-PapersOnLine 54 (2021), pp. 186–191.
[14] A. Brugnoli and D. Matignon, *A port-Hamiltonian formulation for the full von-Kármán plate model*, in *10th European Nonlinear Dynamics Conference (ENOC)*. 2022.
[15] K. Lu, C.E. Augarde, W.M. Coombs, and Z. Hu, *Weak impositions of Dirichlet boundary conditions in solid mechanics: A critique of current approaches and extension to partially prescribed boundaries*, Computer Methods in Applied Mechanics and Engineering 348 (2019), pp. 632–659.
[16] T. Thoma and P. Kotyczka, *Explicit Port-Hamiltonian FEM-Models for Linear Mechanical Systems with Non-Uniform Boundary Conditions*, in *(accepted) 10th Vienna International Conference on Mathematical Modelling*. 2022.
[17] J. Bonet and R.D. Wood, *Nonlinear Continuum Mechanics for Finite Element Analysis*,

Cambridge University Press, 2008.
[18] P. Ciarlet, *Mathematical elasticity*, North-Holland Elsevier Science Publishers, B.V, 1993.
[19] P. Haupt, *Continuum Mechanics and Theory of Materials*, Springer Berlin Heidelberg, 2000.
[20] O.C. Zienkiewicz, R.L. Taylor, and J.Z. Zhu, *The Finite Element Method: Its Basis and Fundamentals*, Butterworth-Heinemann, 2005.
[21] A. Logg, K.A. Mardal, and G.N. Wells, *Automated Solution of Differential Equations by the Finite Element Method*, Springer, 2012.
[22] U. Ayachit, *The ParaView guide: Updated for ParaView version 4.3*, Kitware, 2015.

Appendix A. Tensor calculus

In this section, we recall the most important operations of tensor calculus used in this article. The operations are exemplified by the second order tensors A and B in index notation[6]. This notation is characterized by the indices and uses Einstein summation convention in the following.

$$C = A \cdot B \Rightarrow C_{ij} = A_{ik} B_{kj}$$
$$c = A : B \Rightarrow c = A_{ij} B_{ij}$$

Derivatives with respect to the coordinate X are marked with the help of a comma followed by an index.

$$C = \frac{\partial A}{\partial X} \Rightarrow C_{ijk} = A_{ij,k}$$
$$c = \frac{\partial A}{\partial X} : I \Rightarrow c_i = A_{ij,j}$$

Appendix B. Strong form in vector notation

Before we state (16) in its vector form, the corresponding shapes of some tensors in vector notation are presented. The representation of a tensor in its vector notation based on *Voigt notation* [20] is clarified by an underscore. Considering linear momenta, strains, and their corresponding co-energy variables, we get the transformations:

$$p \in \mathbb{R}^3 \to \underline{p} \in \mathbb{R}^3 \tag{B1}$$
$$v \in \mathbb{R}^3 \to \underline{v} \in \mathbb{R}^3 \tag{B2}$$
$$E \in \mathbb{R}^{3\times 3} \to \underline{E} \in \mathbb{R}^6 \tag{B3}$$
$$S \in \mathbb{R}^{3\times 3} \to \underline{S} \in \mathbb{R}^6 \tag{B4}$$

[6]Since we consider only canonical bases, the specification of the basis can be omitted, so that an index notation is sufficient for the tensor calculus.

The transformation of their time derivatives is identical. The transformation of the deformation gradient and its rate into the vector notation is not so obvious:

$$F \in \mathbb{R}^{3\times 3} \rightarrow \underline{F} \in \mathbb{R}^{9\times 6} \tag{B5}$$

$$\dot{F} \in \mathbb{R}^{3\times 3} \rightarrow \underline{\dot{F}} \in \mathbb{R}^{9} \tag{B6}$$

$$T \in \mathbb{R}^{3\times 3} \rightarrow \underline{T} \in \mathbb{R}^{9} \tag{B7}$$

By introducing the differential operator

$$\underline{D}^T = \begin{bmatrix} \frac{\partial}{\partial X_1} & 0 & 0 & \frac{\partial}{\partial X_2} & 0 & 0 & \frac{\partial}{\partial X_3} & 0 & 0 \\ 0 & \frac{\partial}{\partial X_2} & 0 & 0 & \frac{\partial}{\partial X_3} & 0 & 0 & \frac{\partial}{\partial X_1} & 0 \\ 0 & 0 & \frac{\partial}{\partial X_3} & 0 & 0 & \frac{\partial}{\partial X_1} & 0 & 0 & \frac{\partial}{\partial X_2} \end{bmatrix}, \tag{B8}$$

(16) can be given in its vector notation

$$\begin{bmatrix} \underline{\dot{p}} \\ \underline{\dot{E}} \\ \underline{\dot{F}} \end{bmatrix} = \begin{bmatrix} 0 & \underline{D}^T \underline{F} & \underline{D}^T \\ \underline{F}^T \underline{D} & 0 & 0 \\ \underline{D} & 0 & 0 \end{bmatrix} \begin{bmatrix} \underline{v} \\ \underline{S} \\ \underline{T} \end{bmatrix}, \tag{B9}$$

which makes the formally skew-adjointness even clearer.

Appendix C. Power balance

In this section, the derivation of the power balance is presented in more detail. In particular, the symmetry of the stress tensor is exploited (see Appendix D).

$$\dot{H} = \int_{\Omega_0} \frac{\delta H}{\delta p} \cdot \dot{p} + \frac{\delta H}{\delta E} : \dot{E} + \frac{\delta H}{\delta F} : \dot{F} \, d\Omega_0 \tag{C1}$$

$$= \int_{\Omega_0} v \cdot \dot{p} + S : \dot{E} \, d\Omega_0 \tag{C2}$$

$$= \int_{\Omega_0} v \cdot \mathrm{Div}(F \cdot S) + S : (F^T \cdot \mathrm{Grad}(v)) \, d\Omega_0 \tag{C3}$$

$$= \int_{\Omega_0} -(\mathrm{Grad}(v)^T \cdot F) : S + S : (F^T \cdot \mathrm{Grad}(v)) \, d\Omega_0 + \int_{\partial\Omega_0} v \cdot F \cdot S \cdot N \, d\partial\Omega_0 \tag{C4}$$

$$= \int_{\partial\Omega_0} v \cdot F \cdot S \cdot N \, d\partial\Omega_0, \tag{C5}$$

Appendix D. Characteristic of symmetric tensors

Every second order tensor can be split in a skew-symmetric and symmetric part, accordingly

$$\begin{aligned} &F^T \cdot \mathrm{Grad}(v) = \\ &= \frac{1}{2}(F^T \cdot \mathrm{Grad}(v) + \mathrm{Grad}(v)^T \cdot F) \\ &\quad + \frac{1}{2}(F^T \cdot \mathrm{Grad}(v) - \mathrm{Grad}(v)^T \cdot F). \end{aligned} \tag{D1}$$

Since δS is a symmetric tensor, it follows

$$\begin{aligned} &\delta S : (F^T \cdot \mathrm{Grad}(v)) = \\ &= \delta S : \frac{1}{2}(F^T \cdot \mathrm{Grad}(v) + \mathrm{Grad}(v)^T \cdot F) \end{aligned} \tag{D2}$$

and the skew-symmetric part vanishes. This short explanation shall clarify the derivation of (27b).

Appendix E. Weak form discretization in vector notation

The weak form (33) contains the already introduced vector notation of Appendix A. The virtual variables, which are needed for the weak form, have the same transformation rule as in (B2), (B4) and (B7). Moreover, (33) includes the vector notation of the boundary conditions, elasticity tensor and normal vector:

$$\bar{\tau}_0 \in \mathbb{R}^3 \rightarrow \underline{\bar{\tau}_0} \in \mathbb{R}^3 \tag{E1}$$

$$\bar{\nu} \in \mathbb{R}^3 \rightarrow \underline{\bar{\nu}} \in \mathbb{R}^3 \tag{E2}$$

$$C \in \mathbb{R}^{3\times3\times3\times3} \rightarrow \underline{C} \in \mathbb{R}^{6\times6} \tag{E3}$$

$$N \in \mathbb{R}^3 \rightarrow \underline{N} \in \mathbb{R}^{3\times9} \tag{E4}$$

As already described in Section 3.2, the finite-dimensional system with the matrices

$$\underline{M}_v = \int_{\Omega_0} \underline{\phi}^T \rho_0 \underline{\phi} \, d\Omega_0 \tag{E5}$$

$$\underline{M}_S = \int_{\Omega_0} \underline{\psi}^T \underline{C}^{-1} \underline{\psi} \, d\Omega_0 \tag{E6}$$

$$\underline{M}_F = \int_{\Omega_0} \underline{\theta}^T \underline{\theta} \, d\Omega_0 \tag{E7}$$

$$\underline{Z} = \int_{\Omega_0} \underline{\theta}^T (\underline{D} \, \underline{\psi}) \, d\Omega_0 \tag{E8}$$

$$\underline{K}(\underline{\hat{F}}) = \int_{\Omega_0} (\underline{D} \, \underline{\phi})^T \underline{\theta} \, \underline{\hat{F}} \, \underline{\psi} \, d\Omega_0 - \int_{\Sigma_D} \underline{\phi}^T \underline{N} \, \underline{\theta} \, \underline{\hat{F}} \, \underline{\psi} \, d\Sigma_D \tag{E9}$$

$$\underline{G}_\tau = \int_{\Sigma_N} \underline{\psi}^T \underline{\xi} \, d\Sigma_N \tag{E10}$$

$$\underline{G}_\nu(\underline{\hat{F}}) = \int_{\Sigma_D} \underline{\psi}^T \underline{\hat{F}}^T \underline{\theta}^T \underline{N}^T \underline{\phi} \, d\Sigma_D \tag{E11}$$

$$\tag{E12}$$

can be calculated by means of the weak form (33).